Study on Single Photon Imaging Method for Permanent Shadow Crater of the Moon

Zhongqiu Xia

Beijing Institute of Space Mechanics & Electricity, Beijing 100094, China - xiazhongqiu@126.com

Keywords: Single photon, imaging, permanent shadow crater, the Moon.

Abstract

The detection of the permanent shadow area of the moon is currently a research hotspot. As the name suggests, there is no light in the permanent shadow area, and traditional methods cannot image it. This paper proposes a single photon imaging method that can be used for radiation imaging and distance imaging in this area. A spaceborne photon counting imaging system was designed, a mathematical model for photon counting was derived, and a Monte Carlo simulation method for photon counting process was proposed. The pulse laser echo waveform was simulated, and the radiation performance of the space photon counting imaging system was analysed. The simulated laser echo waveform has a high degree of restoration, indicating that the selected laser repetition rate and gating interval are appropriate. The echo waveforms of targets with the same reflectivity are similar but different, indicating that photon counting is a random process, which is consistent with reality. The higher the target reflectivity, the greater the total number of echo photons. Under the same reflectivity conditions, the total number of echo photons is different but similar. The relative radiation accuracy can reach 0.23%; The laser ranging accuracy can reach 0.075m. This study can provide theoretical basis and technical support for the design of space photon counting imaging systems and the adjustment of in orbit parameters.

1. Introduction

Lunar lava tubes are usually generated by volcanic activity on the moon and are widely distributed in lunar mare and highland areas. Based on the current traces of volcanic activity on the lunar surface, lava tubes beneath the surface may take on different shapes, including cylindrical, elliptical, or irregular shapes, with slopes ranging from 0.4 ° to 6.5 ° and sizes varying from a few meters to several kilometers(Zhou C Y, 2024). Figure 1 shows the remote sensing image and reconstructed three-dimensional structure of the lava tube skylight in the Mare Tranquillitatis area.

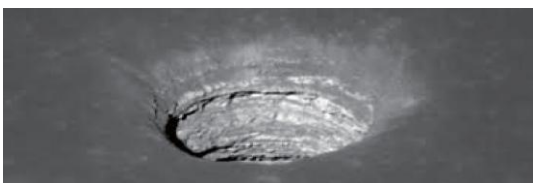

a. Lateral view image(LROC NAC M144395745L)

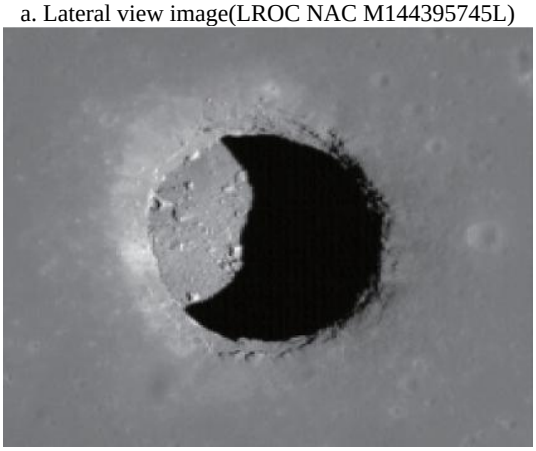

b. Nadir view image(LROC NAC M126710873R)

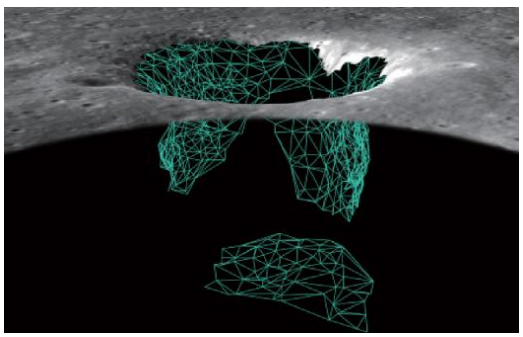

c. Three-dimensional reconstruction model

Fig 1. Lava tube skylight in Mare Tranquillitatis acquired by LRO (Zhou C Y, 2024)

A research team from the University of Trento in Italy used radar data from LRO to discover an expanding tunnel located on the west side of the bottom of the Mare Tranquillitatis crater on the moon. It is speculated that this tunnel may be as long as 30 to 80 meters, with a width of about 45 meters, and the interior may be flat or inclined at a maximum angle of 45 degrees, as shown in fig 2. This significant discovery provides valuable reference for the site selection of future lunar bases.

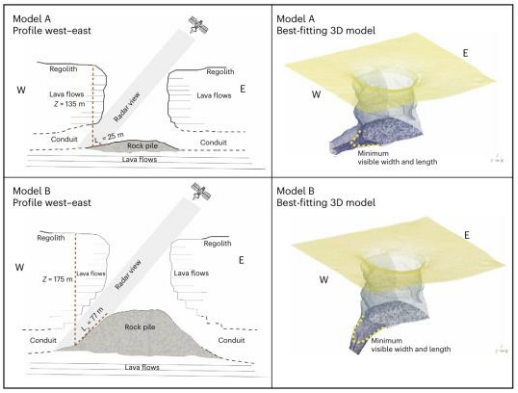

Fig 2. Reconstructed MTP cave conduit based on an inversion of the the Mini-RF radar data. (Carrer L, 2024)

There is no lighting in the permanent shadow area, and current work mainly focuses on three-dimensional geometric reconstruction of the terrain in this area. It is necessary to explore a new imaging method to simultaneously obtain radiation information and geometric information.

In recent years, photon counting imaging technology has developed rapidly. Many researchers have conducted a large number of ground experiments. Ahmed Kirmani et al. proposed a first photon imaging system, which continuously emits laser pulses from pixels at different scanning positions until the first reflected single photon is detected. By recording the number of emitted pulses and the time from departure to detection, intensity and depth features are obtained (Kirmani A, 2014). Genevieve Gariepy et al. proposed ultrafast single photon time-of-flight ranging imaging, using a SPAD array to operate each pixel in a time-dependent single photon counting (TCSPC) mode, thereby obtaining both temporal and spatial information. The time resolution reached 67 picoseconds (Gariepy G, 2015). Jeffrey Shapiro et al. proposed a new type of single photon camera, which uses pulsed laser to illuminate the test scene through a diffuser, and uses an incandescent lamp as the interfering background light. The target and background photons are imaged together through the lens into a single photon avalanche diode array, verifying the interference of background photons on signal photons (Shin D, 2016). Xu et al. broke through the single photon imaging technology at a distance of over 200km, breaking the imaging distance from 10km to the hundred-kilometer level for the first time, reaching 201.5km (Li Z P, 2021).

In order to analyze the radiation performance of space photon counting imaging, this study designed a space photon counting imaging system, established a mathematical model of photon counting, proposed a Monte Carlo simulation method for photon counting process, simulated the pulse laser echo waveform, and analyzed the radiation performance of space photon counting imaging system.

2. Optics

In the process of spaceborne photon counting imaging, the ideal scenario is for all received photons to come from the reflection of the target, without receiving photons from background reflection or radiation and photons reflected or radiated by optical components in the optical system. But the actual situation is not like this. Photons reflected or radiated from the background and photons reflected or radiated from optical components in optical systems always exist. The background mentioned here includes natural scenery, atmosphere, etc (Zhao Y M, 2023). The generation of these photons is difficult to control or can be ignored in small quantities. Therefore, it is necessary to maximize the suppression of photons scattered backwards from optical components in optical systems. A design of an optical system model for backward scattering photon suppression of optical components is shown in the figure 3, mainly composed of pulse laser, 1/4 wave plate, 1/2 wave plate, polarization beam splitter, collimator, polarization maintaining fiber, perforated plane mirror, filter, lens, fiber spectral filter, multimode fiber, single photon detector, and controller. The controller simultaneously sends out trigger signals and gate signals. After receiving the trigger signal, the pulse laser generates monochromatic linearly polarized light, which is modulated by a polarization beam splitter, a 1/4 wave plate, and a 1/2 wave plate combination to emit vertically polarized light. It then passes through a perforated plane mirror and an optical system to reach the target. After diffuse reflection of the target, the vertically polarized light becomes randomly polarized light, which is scattered backwards by the optical element, and the polarization direction remains unchanged, Then, it is filtered by a polarization beam splitter, and only horizontally polarized light can pass through. After receiving the gating signal, the single photon detector finally receives horizontally polarized light reflected from the target, thereby eliminating the influence of backscattered photons from optical components.

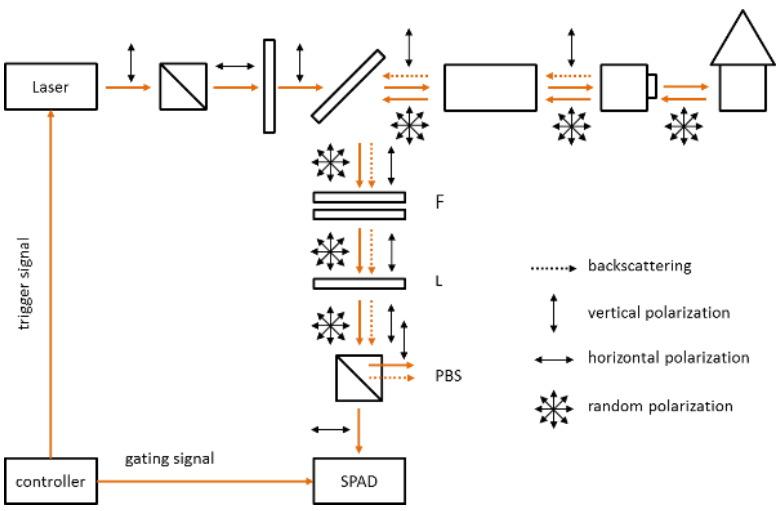

Fig 3. Photon counting imaging system.

3. Counting sensor

The entire process of detecting a photon includes the following steps. Photon injection, where the target signal photon and background photon reach the photosensitive surface of the detector together; Photoelectric conversion, where photons reaching the photosensitive surface are converted into electrons with a certain quantum efficiency, while simultaneously producing shotgun noise electrons; Generating dark noise electrons, generating noise electrons through other means such as thermal current and tunneling current; Electric injection generates avalanche signals with a certain probability for target electrons, background electrons, shotgun noise electrons, and dark noise electrons; Signal detection, where avalanche signals are detected with a certain detection probability and counted for output.

The laser echo signal follows a negative binomial distribution, which can be approximated as a Poisson distribution. Therefore,

within the time interval t of opening the door, the probability of the echo signal producing k photoelectrons is

$$P(k;t) = \frac{N_{electron}(t)^k}{k!} e^{-N_{electron}(t)}, \quad (1)$$

$$N_{electron}(t) = \int_{t_1}^{t_2} \{[n_{signal}(t) + n_{background}(t)] \cdot PDE\} dt, \quad (2)$$

where $N_{electron}(t)$ is the number of echo photoelectrons, $n_{signal}(t)$ is the rate of signal photons, $n_{background}(t)$ is the rate of background photons, t_1 is the start time of the gate control and t_2 is the end time of the gate control. The probability of no photoelectron event occurring during the opening time is

$$P(0;t) = e^{-N_{electron}(t)}, \quad (3)$$

therefore, the probability of at least one photoelectron event generating an avalanche signal and being detected is

$$\overline{P}(0;t) = 1 - e^{-N_{electron}(t)}, \quad (4)$$

the above equation represents the photon count caused by signal photons and background photons.

The probability of shot noise and dark noise causing k photoelectrons during the opening time interval is

$$P_{noise}(k;t) = \frac{N_{noise}(t)^k}{k!} e^{-N_{noise}(t)}, \quad (5)$$

$$N_{noise}(t) = N_{SHOT}(t) + N_{DCR}(t), \quad (6)$$

$$N_{SHOT}(t) = \left\{ \int_{t_1}^{t_2} [n_{signal}(t) \cdot PDE] dt \right\}^{\frac{1}{2}}, \quad (7)$$

$$N_{DCR}(t) = DCR \cdot t, \quad (8)$$

where $N_{noise}(t)$ represents the number of electrons from shotgun noise and other dark noise, $N_{SHOT}(t)$ is the number of shotgun noise electrons, $N_{DCR}(t)$ is the number of dark noise electrons and DCR is the dark counting rate. So the probability of no photoelectron event occurring during the opening time is

$$P_{noise}(0;t) = e^{-N_{noise}(t)}, \quad (9)$$

therefore, the probability of at least one photoelectron event generating an avalanche signal and being detected is

$$\overline{P}_{noise}(0;t) = 1 - e^{-N_{noise}(t)}, \quad (10)$$

the above equation represents the photon count caused by shotgun noise and dark noise.

4. Counting process

A photon counting simulation process is designed as shown in the figure 4. Pulse laser parameters, optical system parameters, and single photon avalanche photodetector parameters are input parameters.

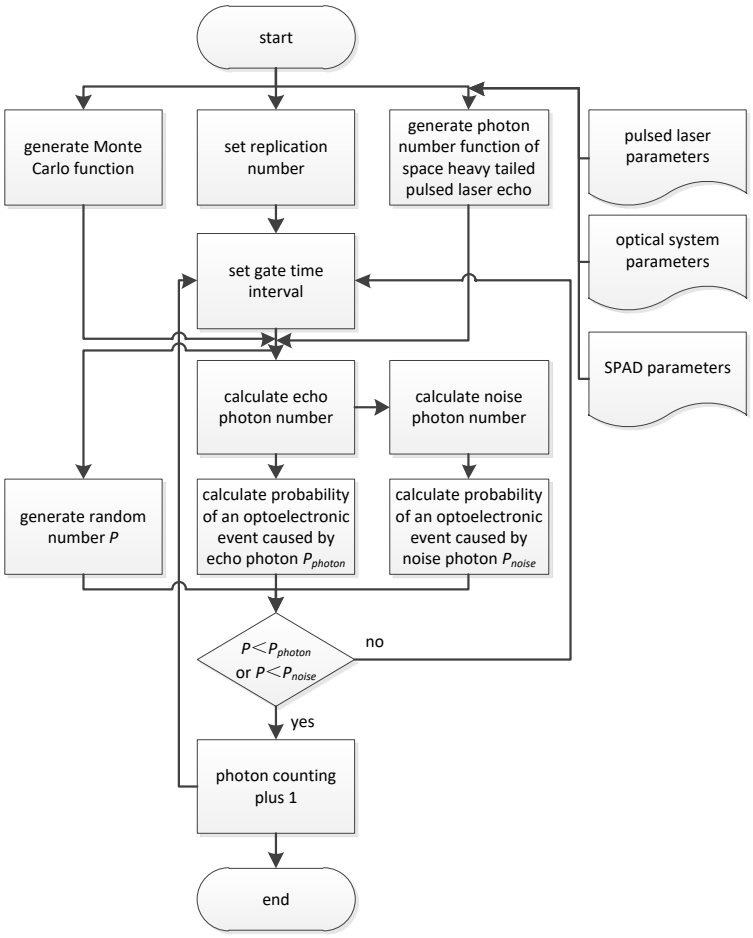

Fig 4. Simulation of counting process.

Based on the spatial heavy tailed pulse laser echo electron number function and Monte Carlo work function, set the number of repetitions, set the gating time t, calculate the echo photoelectron number $N_{electron}(t)$, and then calculate the noise photoelectron number $N_{noise}(t)$. Then, calculate the probability $\overline{P}(0;t)$ and $\overline{P}_{noise}(0;t)$ of at least one photoelectron event caused by the echo photon and at least one photoelectron event caused by the noise electron, and finally generate a random number, Compared with the probability of photon events, when the random number is less than the probability of photoelectron events caused by echo photons or noise, the photon count increases by 1 to enter the dead time. Otherwise, it enters the next gating interval and repeats the operation until the number of repetitions is completed.

5. Results and analysis

The research scenario is set for three targets with reflectivity of 0.9, 0.5, and 0.3 within a detection distance of 15km and a target area range of 23m×23m under no lighting conditions. Considering the feasibility of the project, the laser wavelength is selected as 1550nm, the power density is 1400 W/mm^2, the luminous area is 250μm×250μm, the receiving system focal length is 5m, the F is 9, the SPAD PDE is 0.3, and the dark counting rate is 2000kHz.

The number of echo photons of pulsed laser under different albedos of the target was analyzed using Monte Carlo simulation method, as shown in Figure 5. By comparing the results of the number of echo photons within the same gating time, it can be seen that the higher the target reflectivity, the more echo photons there are, which is consistent with the reality. Due to the long detection distance, the number of target echo photons is very small, reaching the order of 10^{-3}.

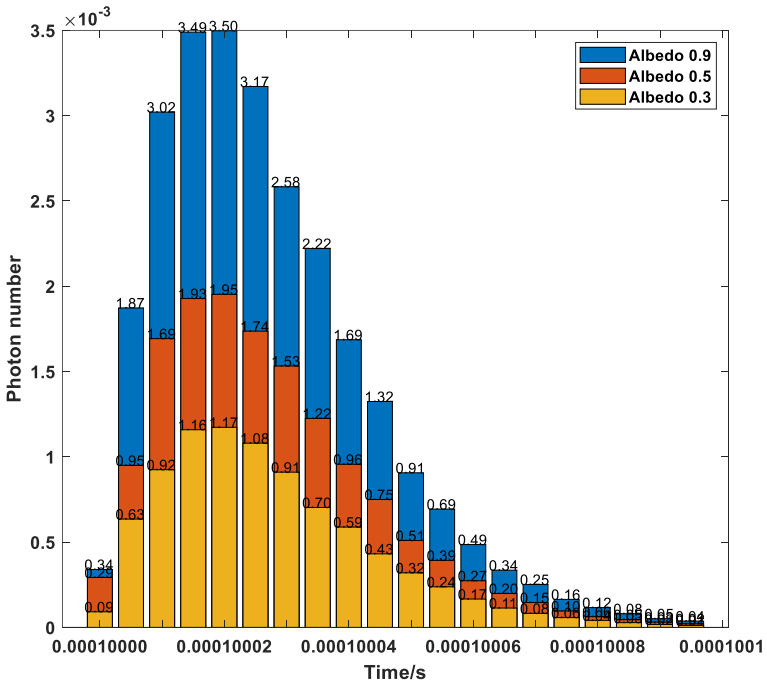

Fig 5. Echo photon number of different albedo.

5.1 Echo waveform

Using the photon counting simulation method, the pulse laser echo waveforms of targets with different reflectivity were simulated three times. The reflected laser waveforms of targets with a reflectivity of 0.3 were obtained as shown in Figures 6 (a) to 6 (c), the reflected laser waveforms of targets with a reflectivity of 0.5 were obtained as shown in Figures 6 (d) to 6 (f), and the reflected laser waveforms of targets with a reflectivity of 0.9 were obtained as shown in Figures 6 (g) to 6 (i). It can be observed that the simulated laser echo waveform has a high degree of restoration, indicating that the selected laser repetition rate and gating interval in this study are appropriate; The echo waveforms of targets with the same reflectivity are similar but different, indicating that photon counting is a random process, which is consistent with reality. Overall, the higher the reflectivity, the higher the photon count.

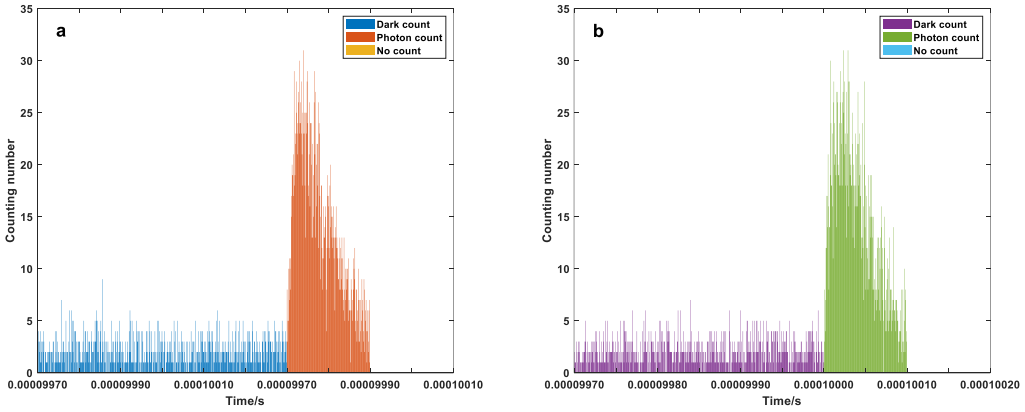

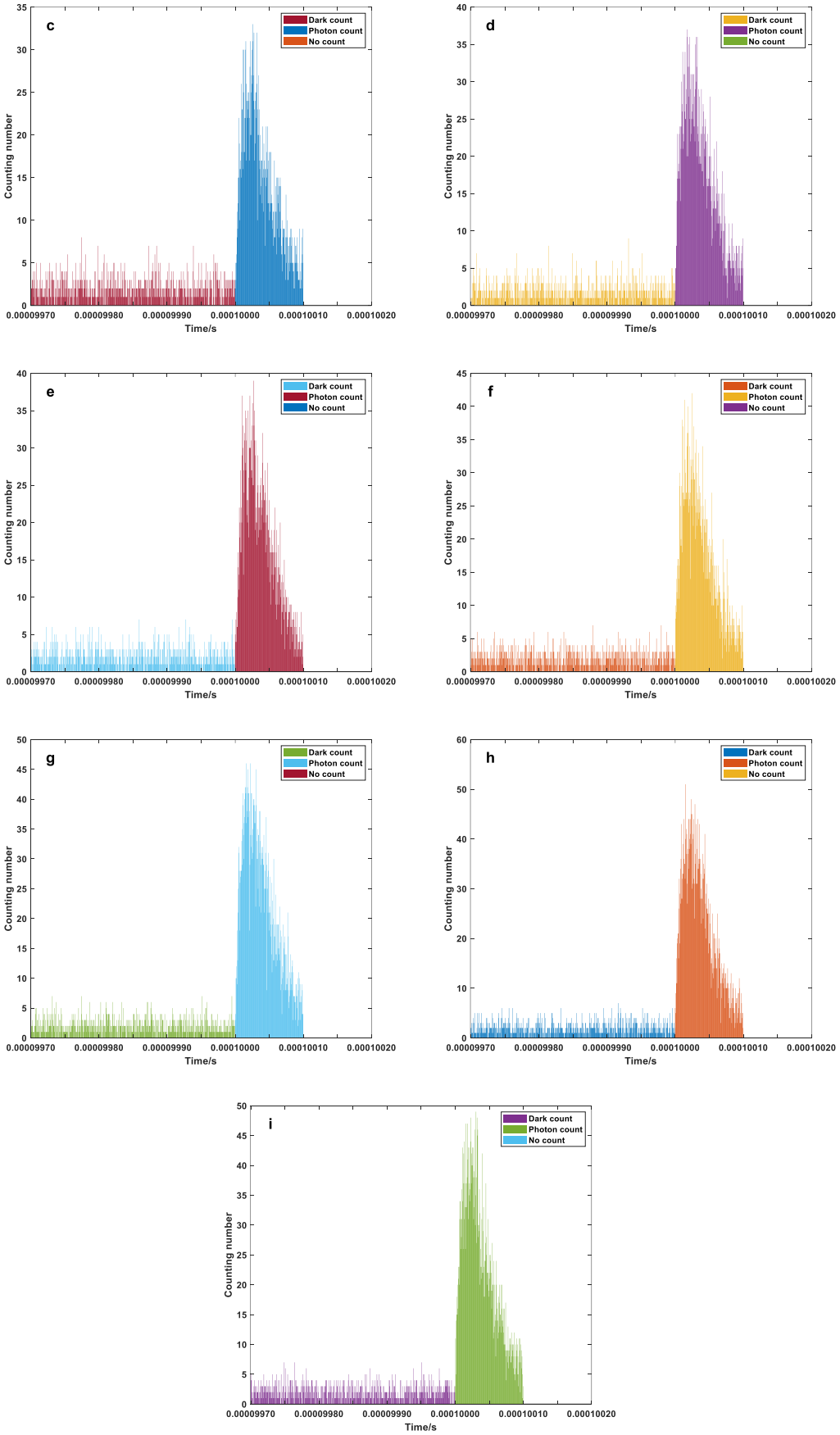

Fig 6. Counting results of different albedo. a-c. Albedo is 0.3. d-f. Albedo is 0.5. g-i. Albedo is 0.9.

5.2 Radiation performence

Another result obtained from simulation is the total number of echo photons under different reflectivity targets, as well as the peak position and corresponding time position of each echo waveform as shown in table 1. By comparing the simulation results of a d g, b e h, and c f i, it can be seen that the higher the target reflectivity, the higher the peak number of echo photons and the total number of echo photons. By comparing the simulation results of a b c, d e f, and g h i, it can be seen that for the same reflectivity, the peak number of echo photons is different but similar, and the total number of echo photons is different but similar. The simulation image is shown in Figure 5. Figure 7 (a) shows the simulation scene, Figure 7 (b) shows the passive imaging simulation results, and Figure 7 (c) shows the photon counting imaging simulation results. The targets that cannot be seen by passive imaging will be displayed. The relative radiation accuracy can reach 0.23%. The positions where different simulation peaks appear are different. If the peak position is used as the judgment position for the echo time, the laser ranging accuracy can reach 0.075m.

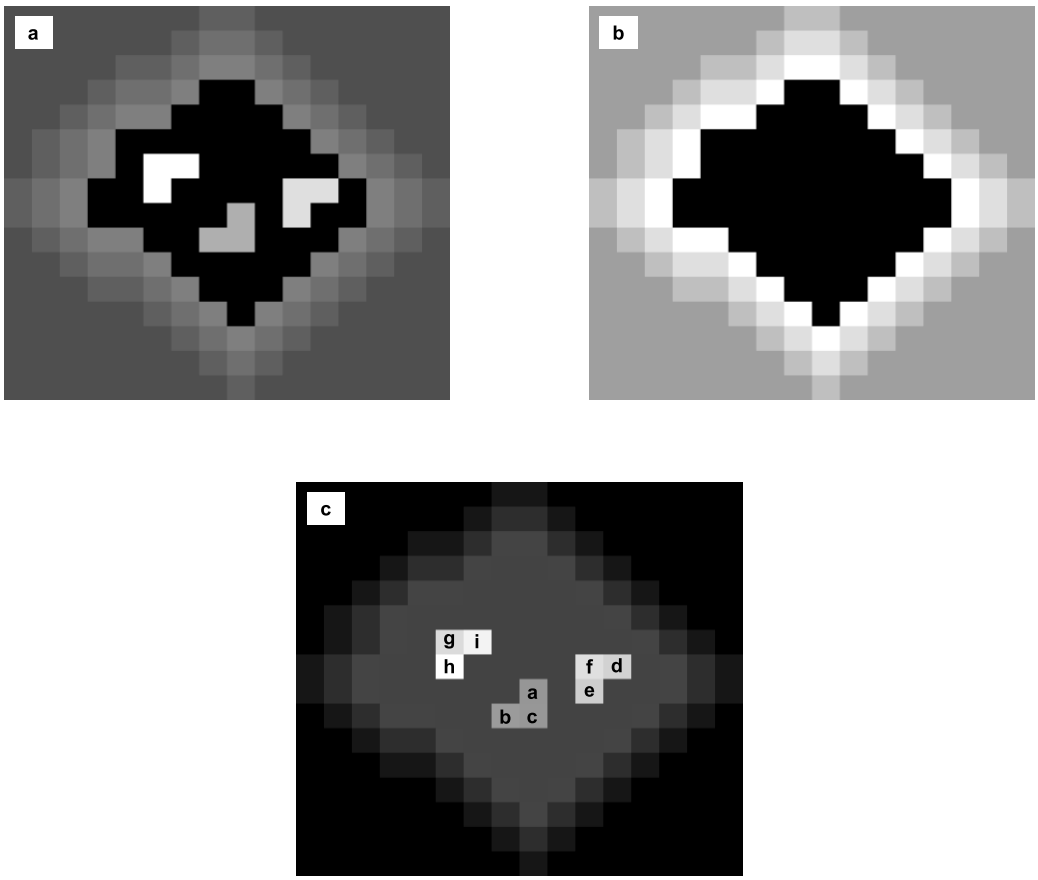

Fig 7. Radiation image. a. Simulation scenario. b. General image by sunlight. c. Photon counting image.

Table 1. Radiation performance of different albedo

No.	Albedo	Peak value	Peak position	Ranging accuracy/m	Counting number
a	0.3	31	40	0.075	2724
b	0.3	31	48	0.525	2751
c	0.3	33	53	0.900	2735
d	0.5	37	36	0.375	3284
e	0.5	39	55	1.050	3225
f	0.5	42	51	0.750	3335
g	0.9	46	34	0.525	4270
h	0.9	51	32	0.675	4291
i	0.9	49	62	1.575	4290

6. Conclusion

In order to solve the problems of long distance and weak illumination in space-based photon counting imaging, a space photon counting imaging system was designed, and a mathematical model of photon counting was derived. A Monte Carlo simulation method for photon counting process was proposed, and the pulse laser echo waveform was simulated. The radiation performance of the space photon counting imaging system was analyzed. By setting reasonable laser repetition rate and gating time, the emission waveform was effectively restored. This research method can simulate the relative radiation accuracy and laser ranging accuracy of photon counting imaging. Subsequent work can introduce atmospheric backscattered photons into the simulation model as background photons to further improve the simulation accuracy of space-based photon counting imaging.

References

Zhou, C.Y., Zhou, M.Y., Xu, Y.S., et al. 2024. Lunar Topographic Survey and Reconstruction and Its Application in Lava Tube Exploration. *Science and Technology Foresight*, 3(1): 34-48. doi.10.3981/j.issn.2097-0781.2024.01.003.

Carrer, L., Pozzobon, R., Sauro, F., et al. 2024. Radar evidence of an accessible cave conduit on the Moon below the Mare Tranquillitatis pit. *Nature Astronomy*, 8, 1119-1126. doi.org/10.1038/s41550-024-02302-y.

Kirmani, A., Venkatraman, D., Shin, D., et al. 2014. First-Photon Imaging. *Science*, 343, 58-61. doi.10.1126/science.1246775.

Gariepy, G., Krstajic, N., Henderson, R., et al. 2015. Single-photon sensitive light-in-flight imaging. *Nature Communications*, 6, 6021. doi.10.1038/ncomms7021.

Shin, D., Xu, F.H., Venkatraman, D., et al. 2016. Photon-efficient imaging with a single-photon camera. *Nature Communications*, 7, 12046. doi.10.1038/ncomms12046.

Li, Z.P., Ye, J.T., Huang, X., et al. 2021. Single-photon imaging over 200km. *Optica*, 8(3), 344-349. doi.org/10.1364/OPTICA.408657.

Zhao, Y.M., Li, F., Pan, C., et al. 2023. Design of space-borne atmospheric detection lidar based on dual-wavelength polarization detection. *Chinese Space Science and Technology*, 6(43), 150-159. doi.10.16708/j.cnki.1000-758X.2023.0094.